Supporting Information

In situ investigation of multicomponent MOF crystallisation during rapid continuous flow synthesis

Brandon He,[a,b] Lauren K. Macreadie,[c,d] James Gardiner,[b] Shane G. Telfer,[d] and Matthew R. Hill*[a,b]

[a.] Department of Chemical Engineering, Monash University, Clayton VIC 3800, Australia

*E-mail: matthew.hill@monash.edu, matthew.hill@csiro.au

[b.] CSIRO Manufacturing, Private Bag 10, Clayton South VIC 3169, Australia

[c.] School of Chemistry, University of Sydney, Sydney NSW 2006, Australia

[d.] MacDiarmid Institute for Advanced Materials and Nanotechnology, Institute of Fundamental Sciences, Massey University, Palmerston North 4442, New Zealand

Contents

1. Experimental Procedure

1.1. Materials

The reagents zinc acetate dihydrate ($Zn(OAc)_2.2H_2O$), terephthalic acid (H_2bdc), 4,4'-biphenyldicarboxylic acid (H_2bpdc), aluminium chloride, acetyl chloride, 1,3,5-triphenylbenzene, sodium hydroxide (NaOH), anhydrous magnesium sulfate ($MgSO_4$), bromine, 1-indanone, magnesium chloride hexahydrate ($MgCl_2.6H_2O$), iron (III) chloride hexahydrate ($FeCl_3.6H_2O$), sodium acetate trihydrate ($NaOAc.3H_2O$) and polyethylene glycol (PEG, Mn = 1400) were purchased from Sigma-Aldrich and used without further purification. The solvents dimethylformamide (DMF), dichloromethane (DCM), ethanol and 1,4-dioxane were of analytical grade and were purchased from Sigma-Aldrich and used as received. 5,5',10,10',15,15'-Hexamethyltruxene-2,7,12-tricarboxylic acid (H_3hmtt) and requisite precursors were synthesised as described in literature.[1, 2]

1.2. Synthesis method

1.2.1. Organic linker synthesis

1,3,5-tri(4,4',4''-acetylphenyl)benzene synthesis[3]

Aluminium chloride (16.66 g, 0.125 mol, 7.8 equiv.) was dissolved in acetyl chloride (90 ml, 1.26 mol, 78.8 equiv.) in a 500 mL flask and stirred for 5 minutes in an ice/water bath. 1,3,5-Triphenylbenzene (5.00 g, 0.016 mol, 1 equiv.) was dissolved in 100 mL dichloromethane (DCM), and slowly added to the $AlCl_3$/acetyl chloride solution. The mixture was then stirred for 2 hours at room temperature, after which the suspension was poured into a 2 L Erlenmeyer flask with at least 1800 mL of ice in it. The mixture was then stirred overnight.

Dichloromethane (100 mL) was added to the mixture before separating the organic and water phases. The water phase was washed with DCM (3 x 100 mL). The three DCM solutions were combined and were washed with 5% NaOH aqueous solution (2 x 100 mL) and dried with anhydrous $MgSO_4$. The solution was evaporated to remove the solvent and a white solid was collected. The solid was finally washed with hot ethanol and air dried overnight and used without further purification (6.71 g, 95 %). ^{1}H NMR (400 MHz, $CDCl_3$, ppm): δ = 2.67 (s, 9H), 8.10 (m, 6H), 7.88 (s, 3H), 7.80 (m, 6H).

4,4',4''-benzene-1,3,5-triyl-tribenzoic acid (H_3btb) synthesis[3]

1,3,5-Tri(4,4',4''-acetylphenyl)benzene (5.0 g, 0.0116 mol, 1 equiv.) was suspended in 250 mL of 1,4-dioxane in a 500 mL flask. Sodium hydroxide (16.0 g, 0.4 mol, 34.5 equiv.) was dissolved in 110 mL of deionised water and chilled in an ice/water bath. Bromine (7.3 mL, 0.1425 mol, 12.3 equiv.) was slowly added to the chilled NaOH solution. The prepared NaOBr solution was added to 1,3,5-tri(4,4',4''-acetylphenyl)benzene suspension and stirred for 2.5 hours at 65 °C. The mixture was cooled to room temperature and a 5% aqueous solution of $Na_2S_2O_3.5H_2O$ was added to the reaction mixture to quench the NaOBr and stirred for 15 minutes. The solution was then filtered and acidified using 50 mL concentrated HCl. The precipitate was filtered and washed with deionised water. The collected product was then recrystallised using hot methanol and collected (5.06 g, 100 %). ^{1}H NMR (400 MHz, DMSO): δ = 8.09 (s, 3H), 8.06 (m, 12H).

Truxene synthesis

1-Indanone (10 g, 0.0757 mol) was dissolved in concentrated HCl (20 mL) and glacial acetic acid (CH_3COOH, 40 mL). The solution was refluxed at 100 °C overnight, after which the solution was cooled and poured on ice. The precipitate was filtered and washed with deionised water followed by acetone. The collected product was then dried and used without further purification (6.83 g, 79 %).: ^{1}H NMR ($CDCl_3$): δ = 8.32 (d, J_1 = 7.5 Hz, 3H), 7.56 (m, 3H), 7.46 – 7.38 (m, 6H), 1.91 (s, 18H).

5,5',10,10',15,15'-hexamethyltruxene-2,7,12-tricarboxylic acid (H3hmtt):
5,5',10,10',15,15'-hexamethyltruxene-2,7,12-tricarboxylic acid (H_3hmtt) was synthesised following literature reported literature procedures.[2] ^{1}H NMR spectra were recorded to verify formation of the desired products.

5,5',10,10',15,15'-hexamethyltruxene: ^{1}H NMR (500 MHz, $CDCl_3$): δ = 1.90 (s, 18H), 7.37 – 7.45 (m, 6H), 7.55 (dd, J_1 = 7.46 Hz, J_2 = 1.54 Hz, 3H), 8.30 (d, J_1 = 8.0 Hz, 3H)

2,7,12-triacetyl-5,5',10,10',15,15'-hexamethyltruxene: ^{1}H NMR (500 MHz, $CDCl_3$): δ = 1.93 (s, 18H), 2.72 (s, 9H), 8.06 (dd, J_1 = 8.3 Hz, J_2 = 1.5 Hz, 3H), 8.17 (d, J_1 = 1.3 Hz, 3H), 8.39 (d, J_1 = 8.5 Hz, 3H)

5,5',10,10',15,15'-hexamethyltruxene-2,7,12-tricarboxylic acid (H_3hmtt): ^{1}H NMR (500 MHz, DMSO):): δ = 1.87 (s, 18H), 8.11 (dd, J_1 = 8.4 Hz, J_2 = 1.6 Hz, 3H), 8.23 (d, J_1 = 1.6 Hz, 3H), 8.40 (d, J_1 = 8.3 Hz, 3H)

1.2.2. MOF synthesis

UMCM-1 synthesis for in situ WAXS experiments
Synthesis of UMCM-1 was performed using a Vapourtec R4 reactor with R2 pump modules. A $Zn(OAc)_2.2H_2O$ solution (5.96 g, 27.2 mmol, 1 equiv.) was prepared in 150 mL DMF. The ligand solution was prepared in DMF (150 mL) containing H_2bdc (1.35 g, 8.1 mmol, 0.3 equiv.) and H_3btb (3.20 g, 7.30 mmol, 0.27 equiv.). The two solutions were each pumped into the reactor at a rate of 0.5 mL/min for a combined flow rate of 1 mL/min. The reaction was conducted at 26 °C and 5 bar pressure.

MUF-7a synthesis for in situ WAXS experiments
Synthesis of MUF-7a was performed using a Vapourtec R4 reactor with R2 pump modules. A $Zn(OAc)_2.2H_2O$ solution (3.47 g, 15.8 mmol, 1 equiv.) was prepared in DMF (150 mL). The ligand solution was prepared in DMF (150 mL) containing H_2bdc (0.37 g, 2.25 mmol, 0.14 equiv.), H_2bpdc (0.55 g, 2.25 mmol, 0.14 equiv.) and 0.0252 M H_3btb (1.64 g, 3.75 mmol, 0.23 equiv.). The two solutions were pumped into the reactor at a rate of 0.5 mL/min for a combined flow rate of 1 mL/min. The reaction was performed at 26 °C and 80 °C at 5 bar pressure.

1.2.3. $MgFe_2O_4$ nanoparticle synthesis

$MgCl_2.6H_2O$ (1.02 g, 5 mmol) and $FeCl_3.6H_2O$ (2.7 g, 10 mmol) was dissolved in ethylene glycol (80 mL) along with sodium acetate trihydrate ($NaOAc.3H_2O$, 7.2 g, 52.9 mmol) and polyethylene glycol (PEG, Mn = 1500, 4 g,). The mixture was heated under reflux for 16 hours, with the precipitate collected using a magnet. The solid product was washed thoroughly with distilled water (3 x 40 mL), followed by ethanol (3 x 40 mL). The solid was then dried at 90 °C under vacuum for 24 hours to yield a black powder.[4]

1.3. Characterisation

1.3.1. ^{1}H Nuclear magnetic resonance spectroscopy

^{1}H NMR spectra of samples were obtained either from Bruker Avance 400 spectrometer or Avance 500 spectrometer operating at 400 mHz and 500 mHz respectively. Base digestions of MOF samples were performed using a mixture of sodium deuteroxide (NaOD) solution in deuterated water (D_2O) with DMSO-d_6.

UMCM-1:

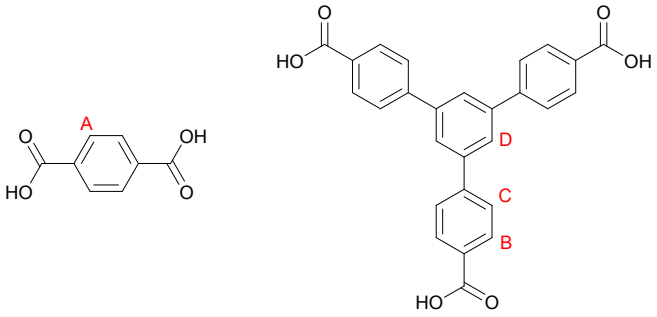

Reaction 1: ^{1}H NMR (500 MHz, DMSO, ppm) δ = 7.74 (m, 13.7H, H^A, H^C), 7.87, (s, 4H, H^D), 7.95 (d, J_1 = 8.3 Hz, 8.2H, H^B). Mass yield: 106.9 mg

Reaction 2: ^{1}H NMR (500 MHz, DMSO, ppm) δ = 7.74 (m, 13.9H, H^A, H^C), 7.88, (s, 4H, H^D), 7.97 (d, J_1 = 8.0 Hz, 8.5H, H^B). Mass yield: 95.8 mg

Reaction 3: ^{1}H NMR (500 MHz, DMSO, ppm) δ = 7.76 (m, 14.8H, H^A, H^C), 7.90, (s, 4H, H^D), 7.93 (d, J_1 = 8.4 Hz, 8.4H, H^B). Mass yield: 83.9 mg

Reaction 4: ^{1}H NMR (500 MHz, DMSO, ppm) δ = 7.75 (m, 15.0H, H^A, H^C), 7.88, (s, 4H, H^D), 7.92 (d, J_1 = 8.6 Hz, 8.1H, H^B). Mass yield: 79.2 mg

Reaction 5: ^{1}H NMR (500 MHz, DMSO, ppm) δ = 7.75 (m, 14.1H, H^A, H^C), 7.87, (s, 4H, H^D), 7.94 (d, J_1 = 8.2 Hz, 8.1H, H^B). Mass yield: 91.0 mg

Reaction 6: ^{1}H NMR (500 MHz, DMSO, ppm) δ = 7.74 (m, 13.3H, H^A, H^C), 7.87, (s, 4H, H^D), 7.96 (d, J_1 = 8.4 Hz, 8.0H, H^B). Mass yield: 120.5 mg

MUF-77-methyl

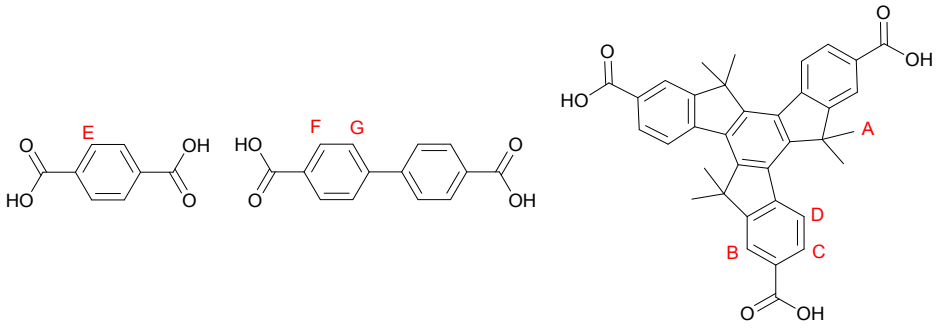

Reaction 1: ^{1}H NMR (500 MHz, DMSO, ppm) δ = 1.77, (s, 24.7H, H^A), 7.59 (d, J_1 = 8.39 Hz, 1.98H, H^G), 7.72, (s, 2.2H, H^E), 7.88 (d, J_1 = 8.39 Hz, 2.1H, H^F), 7.91, (dd, J_1 = 8.14 Hz, J_2 = 1.02 Hz, 4.3H, H^C), 8.07, (s, 4.2H, H^B), 8.19, (d, J_1 = 8.14 Hz, 4H, H^D). Mass yield: 115.2 mg

Reaction 2: ^{1}H NMR (500 MHz, DMSO, ppm) δ = 1.80, (s, 25.6H, H^{A}), 7.55 (d, J_1 = 8.39 Hz, 2.2H, H^{G}), 7.71, (s, 2.4H, H^{E}), 7.90 (d, J_1 = 8.39 Hz, 2.4H, H^{F}), 7.93, (dd, J_1 = 8.14 Hz, J_2 = 1.34 Hz, 4.3H, H^{C}), 8.08, (s, 4.2H, H^{B}), 8.15, (d, J_1 = 8.39 Hz, 4H, H^{D}). Mass yield: 137.2 mg

Reaction 3: ^{1}H NMR (500 MHz, DMSO, ppm) δ = 1.78, (s, 23.3H, H^{A}), 7.58 (d, J_1 = 8.59 Hz, 1.9H, H^{G}), 7.7, (s, 2.2H, H^{E}), 7.88 (d, J_1 = 8.39 Hz, 1.9H, H^{F}), 7.92, (dd, J_1 = 8.20 Hz, J_2 = 1.60 Hz, 4.4H, H^{C}), 8.07, (s, 4.1H, H^{B}), 8.17, (d, J_1 = 8.39 Hz, 4H, H^{D}). Mass yield: 41.2 mg

Reaction 4: ^{1}H NMR (500 MHz, DMSO, ppm) δ = 1.78, (s, 23.9H, H^{A}), 7.59 (d, J_1 = 8.14 Hz, 2.3H, H^{G}), 7.74, (s, 2.1H, H^{E}), 7.90 (d, J_1 = 8.14 Hz, 2.0H, H^{F}), 7.93, (d, J_1 = 8.14 Hz, 3.9H, H^{C}), 8.09, (s, 3.9H, H^{B}), 8.19, (d, J_1 = 7.86 Hz, 4H, H^{D}). Mass yield: 47.4 mg

Reaction 5: ^{1}H NMR (500 MHz, DMSO, ppm) δ = 1.79, (s, 24.5H, H^{A}), 7.59 (d, J_1 = 8.17 Hz, 2.3H, H^{G}), 7.74, (s, 2.1H, H^{E}), 7.90 (d, J_1 = 8.45 Hz, 1.9H, H^{F}), 7.93, (d, J_1 = 8.14 Hz, 3.9H, H^{C}), 8.09, (s, 4.0H, H^{B}), 8.19, (d, J_1 = 8.14 Hz, 4H, H^{D}). Mass yield: 198.0 mg

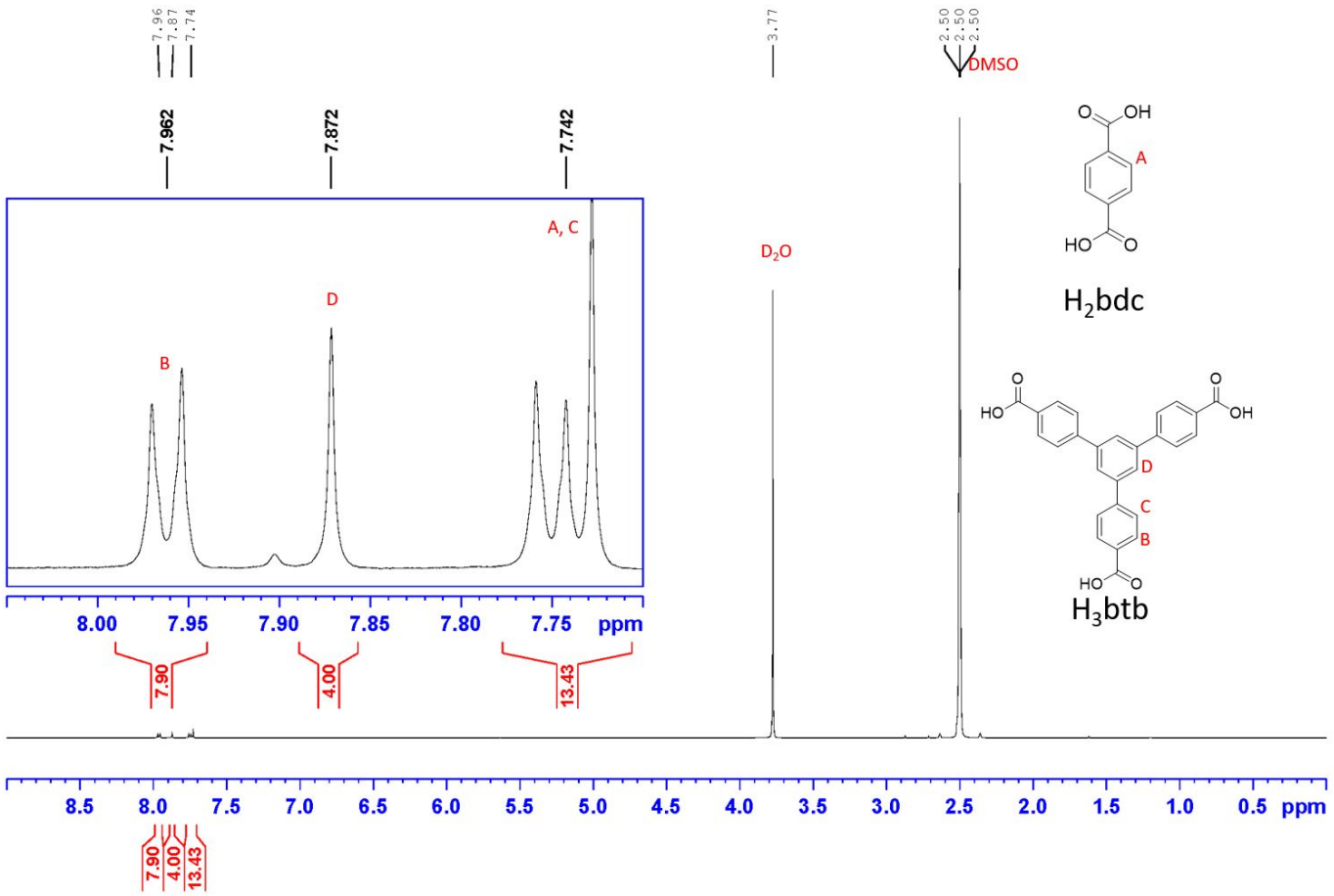

Figure S1. Example ^{1}H NMR spectrum of digested UMCM-1.

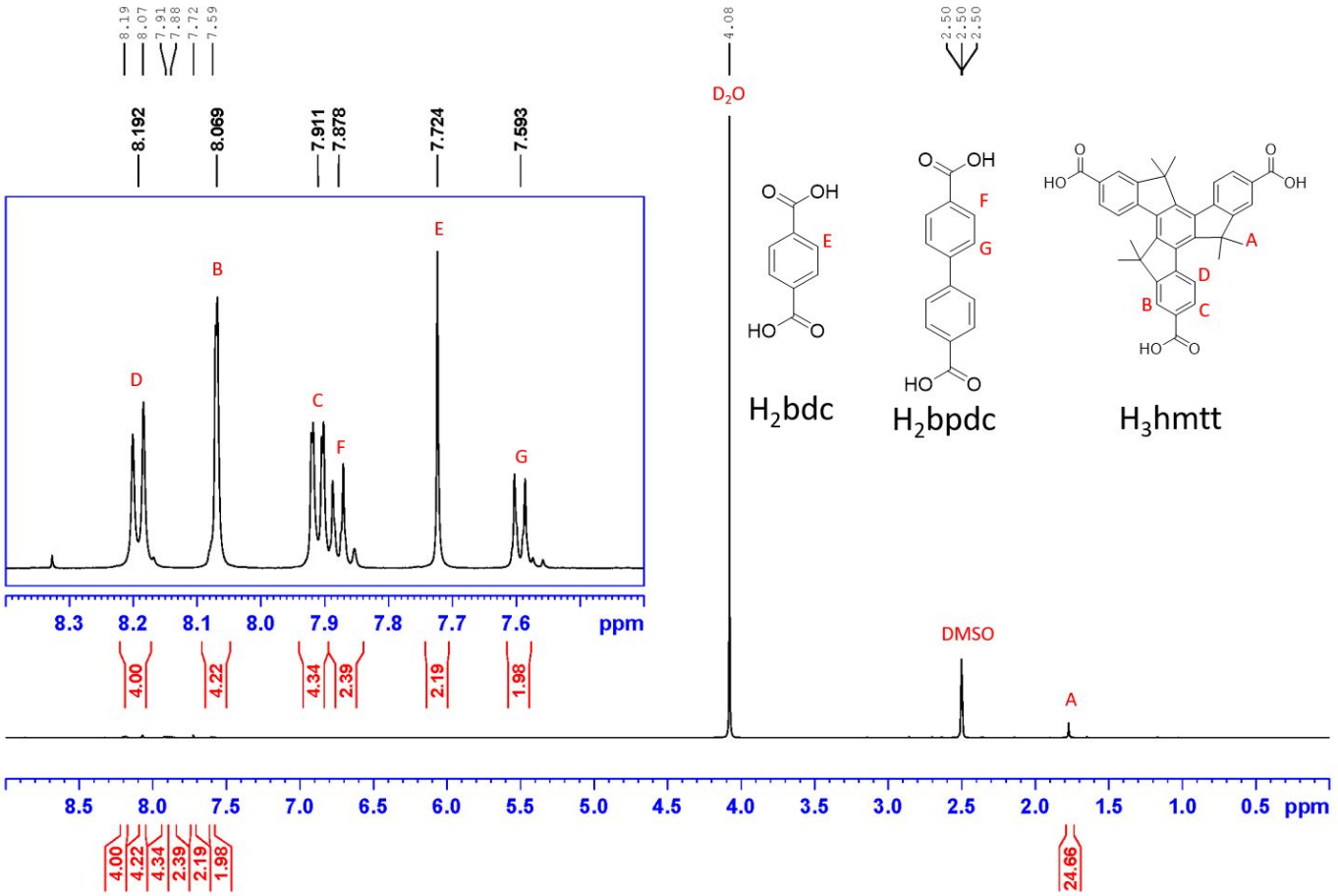

Figure S2. Example ^{1}H NMR spectrum of base digested MUF-77-methyl.

1.3.2. Powder X-ray diffraction

UMCM-1 powder samples were mounted on zero background holders with petroleum jelly (X-alliance GMBH) or DMF where stated to mitigate the effects of moisture during data acquisition due to the moisture sensitivity of the MOF. MUF-77 powder samples were dry mounted on zero background holders for analysis. Powder X-ray diffraction (PXRD) was performed using a Bruker D8 diffractometer with Copper Kα1 radiation (λ=1.54060, 40 kV, 40 mA) and LynxEye as the detector. The powder diffraction patterns were obtained in the 2θ range of 3 ° – 85 °.

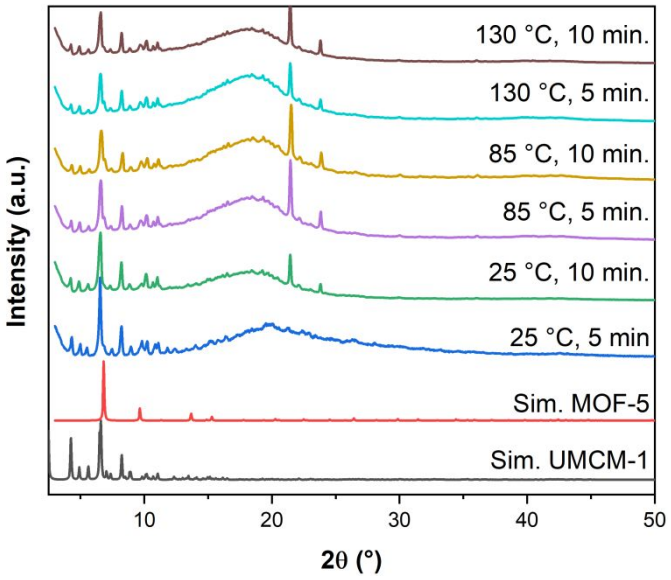

Figure S3. PXRD of UMCM-1. Note: PXRD of 25 °C, 5 min. was performed with DMF present instead of petroleum jelly.

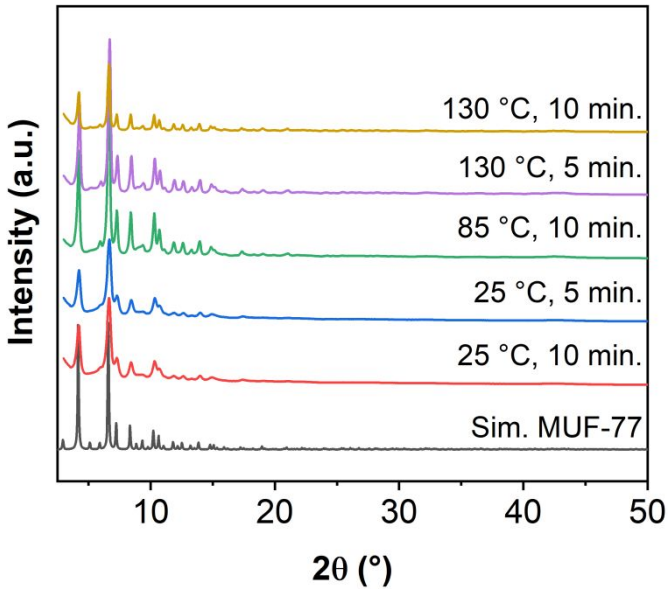

Figure S4. PXRD of MUF-77-methyl.

1.3.3. Thermogravimetric analysis

Thermogravimetric analysis (TGA) was performed using a Mettler Toledo TGA 2 thermogravimetric instrument. The temperature range used was 25 °C to 850 °C at a ramp rate of 5 °C/min under a nitrogen flow rate of 20 mL/min.

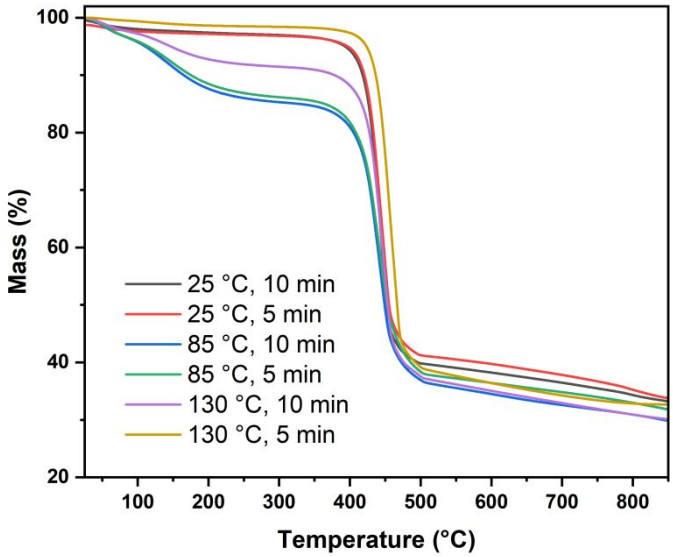

Figure S5. TGA plot of UMCM-1.

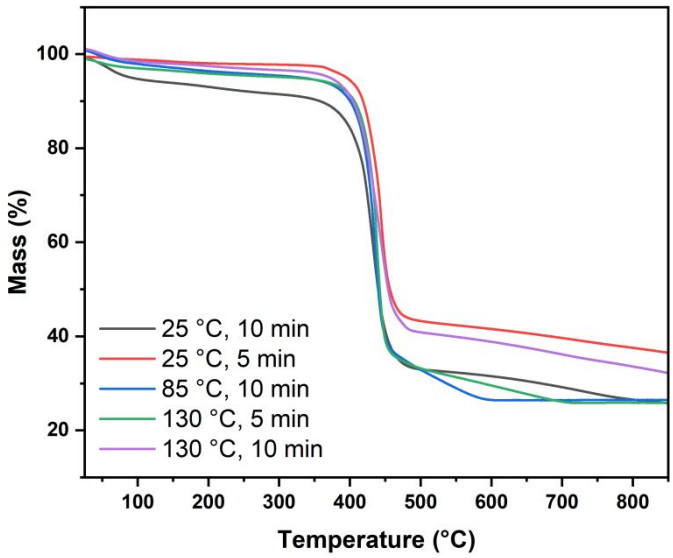

Figure S6. TGA plot of MUF-77-methyl.

1.3.4. Gas sorption, surface area and pore size analysis

Gas sorption characterisation was performed on Micromeritics ASAP 2420. UHP-grade (99.999% purity) N_2 was used for N_2 sorption measurements. Samples were transferred into pre-weighed analysis tubes which were capped with seal frits. UMCM-1 samples were activated at 120 °C for 10 hours under vacuum. MUF-77 samples were activated at 80 °C for 24 hours under vacuum. The degassed and activated samples were weighed to determine the mass of MOF within the analysis tubes. N_2 isotherms in the range of 0 – 1 bar for samples were obtained at 77 K in a liquid nitrogen bath.

Vapour sorption characterisation was performed on a Micromeritics 3Flex. 2,3-Dimethylbutane (purchased from Sigma-Aldrich) was loaded into the instrument via the vapour sorption attachment. Samples were transferred into pre-weighed analysis tubes which were capped with seal frits and activated at 80 °C for 24 hours under vacuum. The degassed and activated samples were weighed to determine the mass of MOF within the analysis tubes. 2,3-Dimethylbutane isotherms in the range of 0 – 0.27 bar were obtained at 298 K in a water bath.

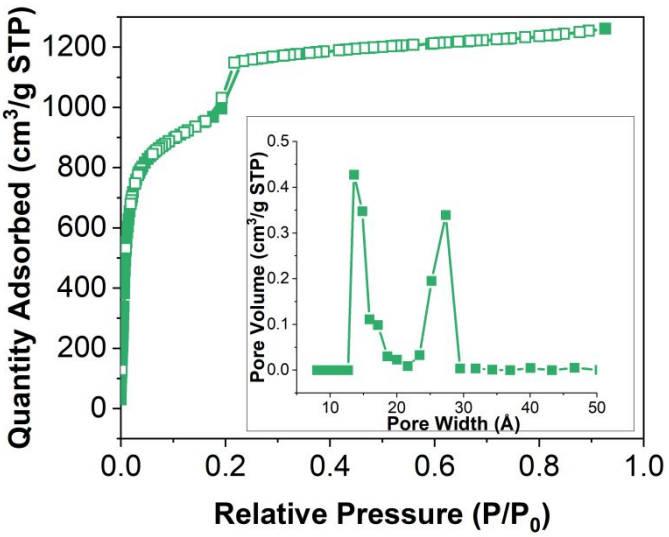

Figure S7. N_2 gas sorption isotherm at 77 K for UMCM-1 synthesised at 130 °C. (inset) Pore size distribution for flow-UMCM-1.

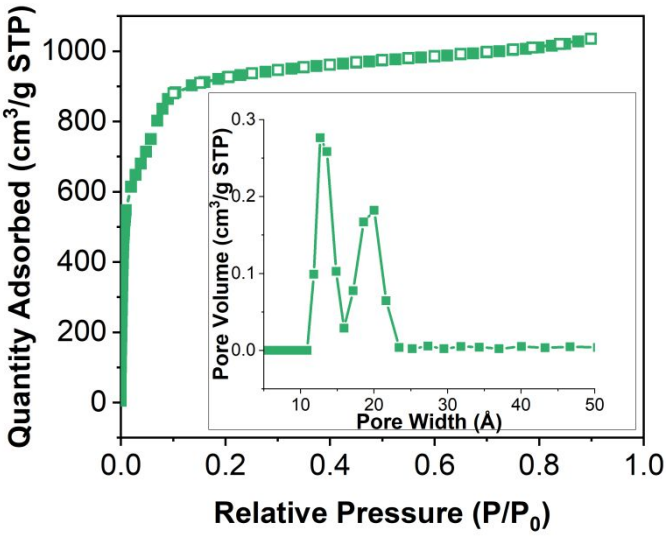

Figure S8. N_2 gas sorption isotherm at 77 K for MUF-77-methyl synthesised at 130 °C. (inset) Pore size distribution for flow-MUF-77.

1.3.5. Scanning electron microscopy

Scanning electron microscopy (SEM) was conducted using a JEOL 7001F FEGSEM for secondary electron imaging and Energy Dispersive X-ray spectroscopy (EDX). The MOF samples were mounted onto silicon substrates by pipetting dilute MOF suspensions in DCM and allowing the DCM to evaporate. Samples are coated with iridium for microscopy.

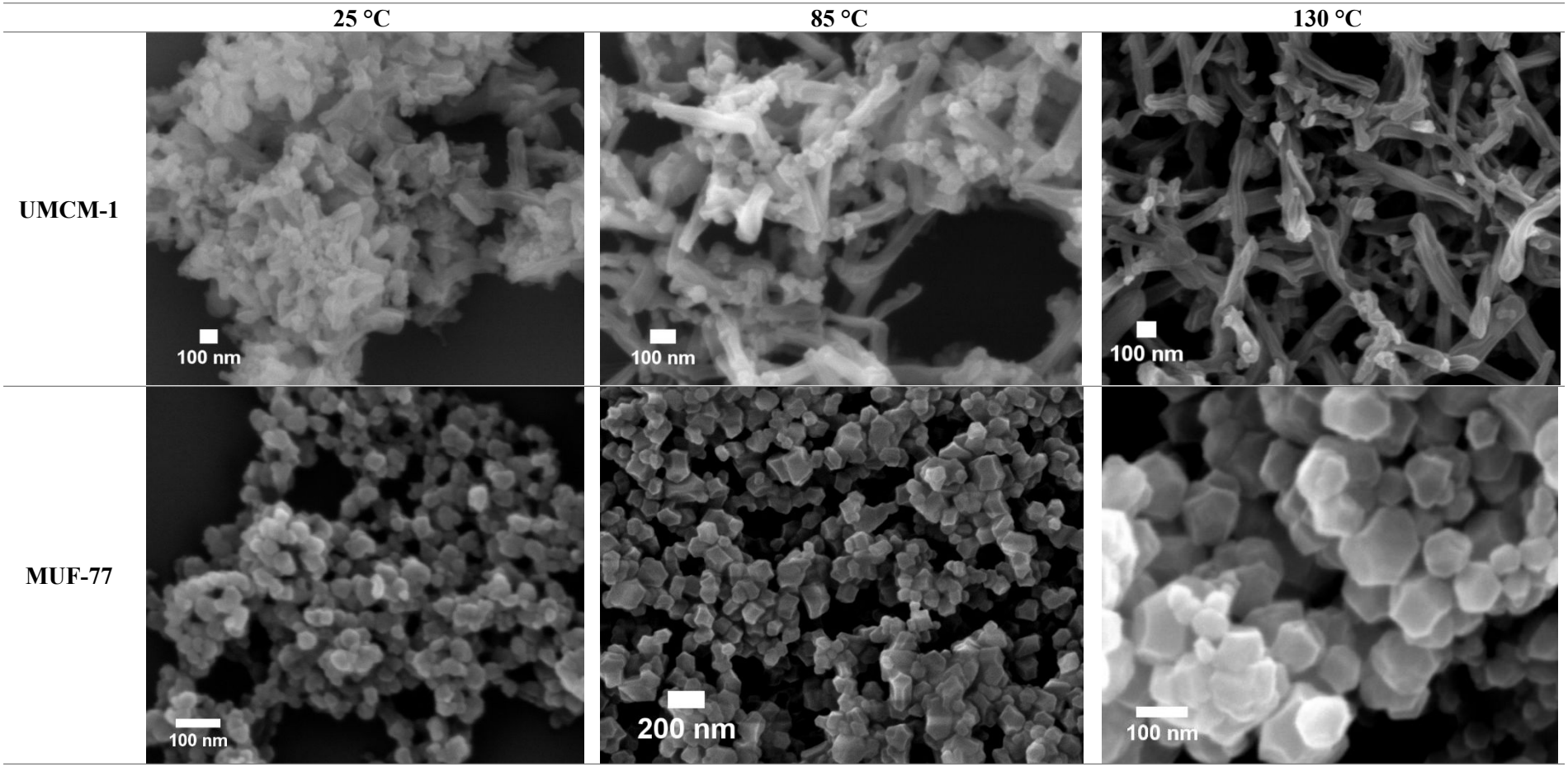

Figure S9. SEM micrographs of UMCM-1 and MUF-77 at various reaction temperatures.

1.4. Crystal Structures

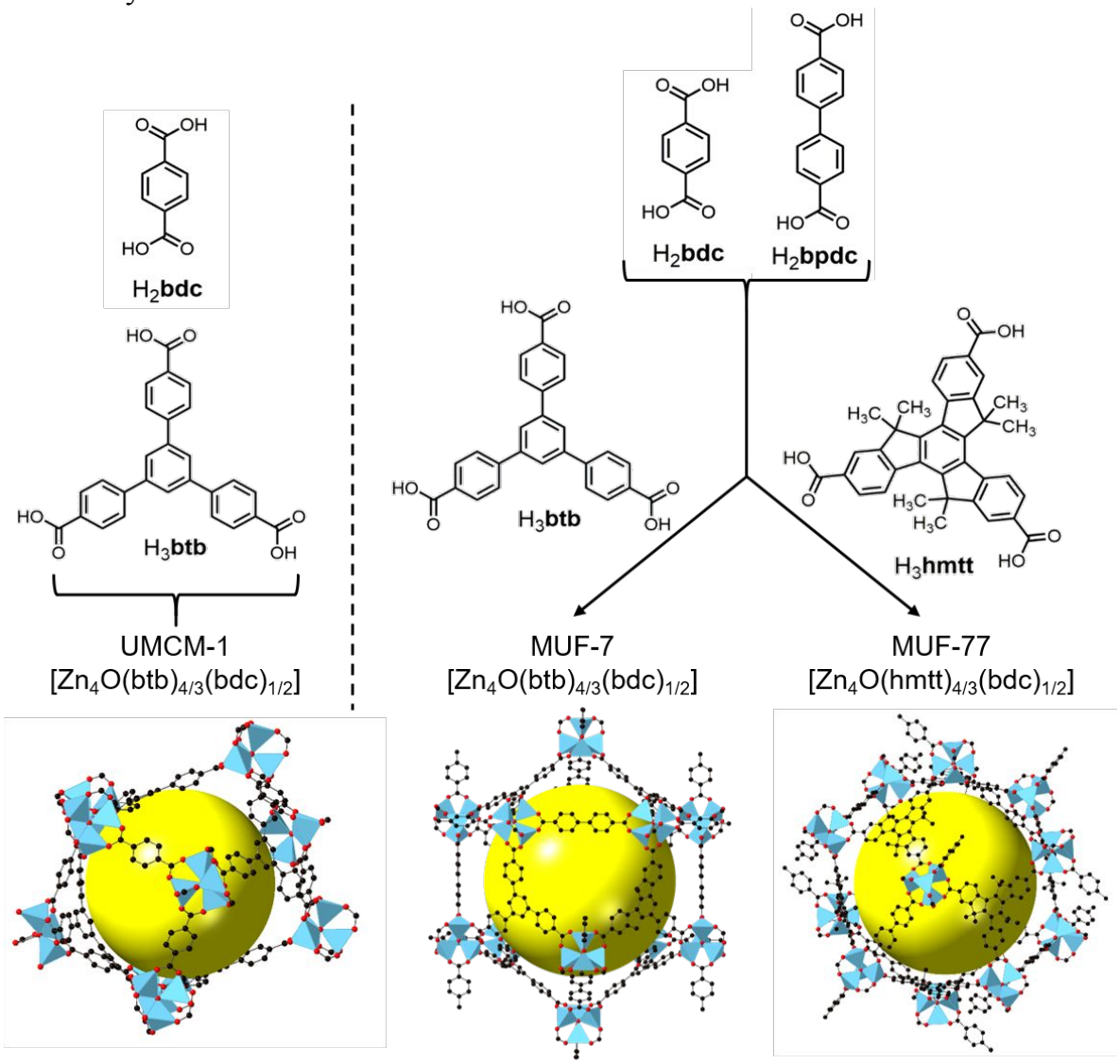

Figure S10. Crystal structures of UMCM-1 and MUF-77 series with their constituent linkers and mesopores highlighted.

2. *In situ* wide-angle X-ray scattering

2.1. Experimental setup

In situ wide-angle X-ray scattering (WAXS) was performed on the SAXS beamline at the Australian Synchrotron in transmission mode at an energy of 11.5 keV (λ = 1.000 Å) with an unfocused and collimated x-ray beam with size of 0.25 x 0.45 mm^2. Diffraction patterns were collected with a Pilatus 2M detector which was positioned at a distance of 742 mm providing a q range of 0.020 $Å^{-1}$ to 1.716 $Å^{-1}$.

The experimental set up and sample cell was constructed with the parts described in **Table S1.** The construction of the sample cell (**Figure S11)** was to adapt and connect the sample environment, quartz capillary, to the reactor system and the backpressure regulator downstream. Tuohy Borst adapters with O-rings were used to provide pressure fittings and adapt to screw type threads to enable reactor tubing to be attached. Adapters threaded through the brackets mounted onto extruded aluminium enabled mounting to the optical breadboard table at the beamline, provided the mechanical rigidity to the cell and enabled the sample cell to hold pressures up to 10 bar. PFA tubing of known lengths (**Table S2**) were connected to the sample cell to obtain the various time point diffraction patterns. The reaction method performed for the *in situ* study are outlined in page 4. Above-ambient temperature (80 °C) reactions were conducted using the glass enclosures connected to the Vapourtec R4 reactor unit.

Table S1. Parts list for *in situ* WAXS experimental apparatus.

Part	Description	Manufacturer
40089-20	Double Funnel mark tubes Quartz Funnel Diameter 3 mm Midsection diameter 1 mm	Hilgenberg
316-1032-TUOHY-3	7-9 Fr Tuohy Borst Adapter to 10-32 Male Thread	Microgroup
P-669-01	Stainless Steel 1/8” 10-32 Female to ¼-28 Male adapter	IDEX
P-703	PEEK 1/8” 1/4-28 Union	IDEX
	1/16” OD PFA Tubing	VICI Jour
R2+	Pump	Vapourtec
R4	Reactor Unit	Vapourtec
SS-4R3A	Backpressure Regulator	Swagelok

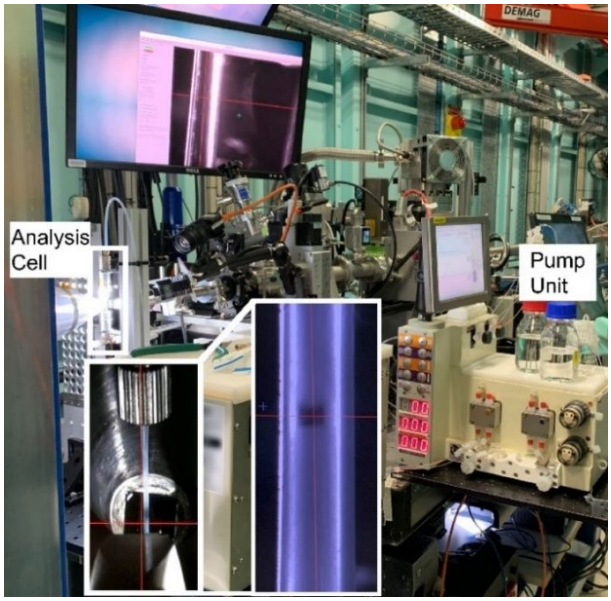

Figure S11. *In situ* WAXS experimental set up. (Inset) magnified view of the sample cell in line with the beam

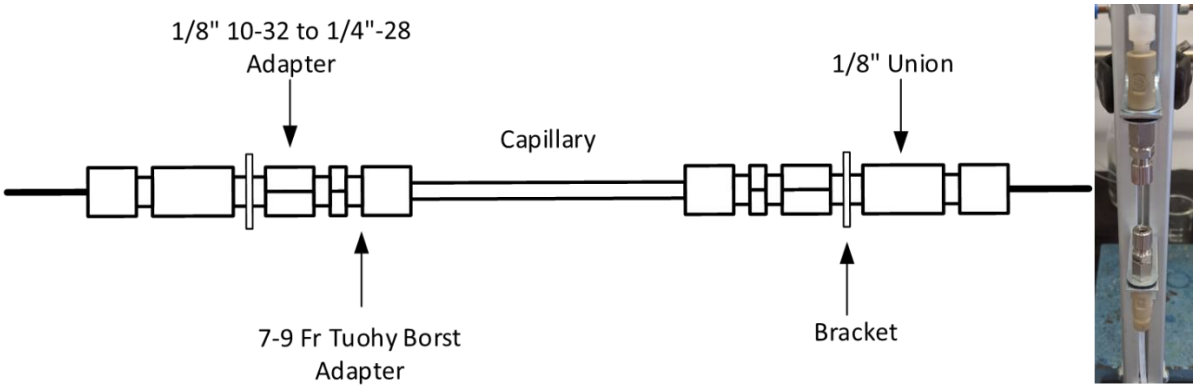

Figure S12. (Left) Schematic of the sample cell. (Right) Enlargement of the assembled sample cell.

Table S2. Reactor tubing length and equivalent total residence time for a total flow rate of 1 mL/min.

Length (mm)	Time (s)
0	6.2
81	10
293	20
505	30
823	45
1142	60
1778	90
3663	180
5598	270
8650	420
12601	600

2.2. Data analysis

Diffraction patterns were obtained which were reduced using ScatterBrain, and a conversion was applied to the data to convert q (x-axis) into 2θ. Bragg peaks were identified, with the intensities obtained, plotted and fitted to Avrami-Erofe'ev (AE) and Finke-Watzky (FW) models.[5-7]

Each model was fitted using nonlinear least squares curve fitting on OriginPro 2018. The Avrami-Erofe'ev model describes the transformation of solid particles and is expressed as:

$$\alpha = 1 - e^{-(kt)^n} \quad (1)$$

Where α is the extent of crystallization, k is the rate constant (s^{-1}), t is time (s) and n is the crystal growth exponent. The value of crystal growth exponent describes the growth regime where values lying within specific ranges. Crystal growth exponent values between 0.54 – 0.62 indicate a diffusion-controlled mechanism, values between 1.00 – 1.24 indicate first-order boundary-controlled mechanism and values between 2.00 – 3.00 indicate a mechanism controlled by nucleation and growth.[8]

The Finke-Watzky model is a two-step kinetic model that deconvolutes the rate constant into two specific rates: nucleation and growth. This model is expressed as:

$$\alpha = 1 - \frac{k_1 + k_2}{k_2 + k_1 \exp\left[(k_1 + k_2)t\right]} \quad (2)$$

Where α is the extent of crystallisation, k_1 is the nucleation rate constant (s^{-1}), k_2 is the autocatalytic growth rate constant ($M^{-1} \cdot s^{-1}$) and t is time (s).

Crystallite sizes were calculated by the Scherrer equation.

$$D = \frac{\kappa\lambda}{\beta cos\theta}$$

Where D is the mean crystallite size, κ is the dimensionless shape factor (assumed to be 0.9), λ is the X-ray wavelength in Angstroms, β is the full width at half maximum intensity (FWHM) and θ is the Bragg angle.

FWHMs for each reaction time point were obtained from the diffraction patterns using OriginPro 2018 peak fitting which were then used in the Scherrer equation to calculate the crystallite sizes.

Table S3. Kinetic parameters for UMCM-1.

	AE Model					FW Model				
Bragg Peak	**k (s^{-1})**	**k error**	**n**	**n error**	**R^2**	**k_1 (s^{-1})**	**k_1 error**	**k_2 ($M^{-1} \cdot s^{-1}$)**	**k_2 error**	**R^2**
(010)	0.00438	3.14E-04	1.674	0.244	0.973	0.00147	5.02E-04	0.01008	0.0029	0.977
(111)	0.00587	6.59E-04	1.047	0.136	0.955	0.00488	0.00123	0.00269	0.00369	0.957

The AE crystal growth exponent, n, of 1.7 was obtained for the (010) reflection of UMCM-1 compared to an n value of 1 for (111) indicating a difference in growth limitation where the [010] direction is

limited by nucleation and growth compared to [111] being phase boundary limited (rate-limited by the surface reaction).

Table S4. Kinetic parameters for MUF-7 at 26 °C and 80 °C.

		AE Model					FW Model				
	Bragg Peak	**k (s^{-1})**	**k error**	**n**	**n error**	**R^2**	**k_1 (s^{-1})**	**k_1 error**	**k_2 ($M^{-1}\cdot s^{-1}$)**	**k_2 error**	**R^2**
26 °C	**(022)**	0.00284	3.1E-04	1.43	0.29	0.929	0.00145	6.6E-04	0.0043	0.0028	0.923
	(042)	0.00272	2.7E-04	1.47	0.28	0.936	0.00128	5.3E-04	0.0046	0.0024	0.935
	(422)	0.00279	3.0E-04	1.40	0.28	0.938	0.00146	6.2E-04	0.0041	0.0026	0.927
80 °C	**(022)**	0.00705	1.4E-03	0.87	0.21	0.871	0.00915	0.00304	-0.0051	0.0070	0.876
	(042)	0.00701	1.2E-03	0.94	0.19	0.912	0.00823	0.00243	-0.0032	0.0061	0.915
	(422)	0.00684	1.1E-03	0.89	0.17	0.914	0.00858	0.00235	-0.0043	0.0056	0.918

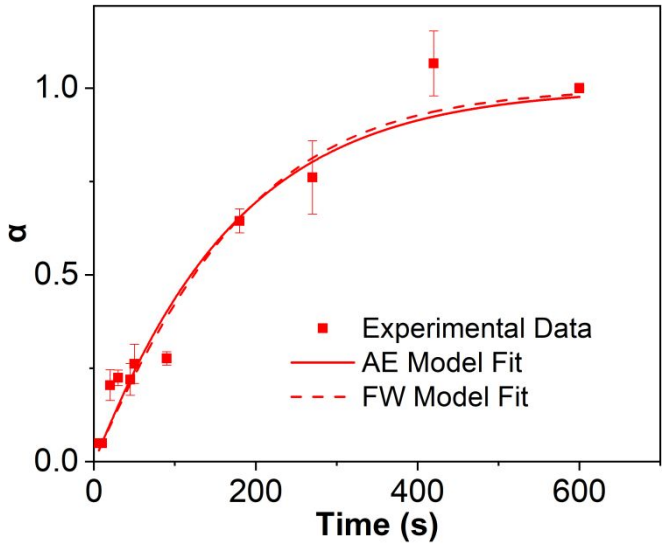

Figure S13. Extent of crystallisation over time for UMCM-1 for the (111) reflection.

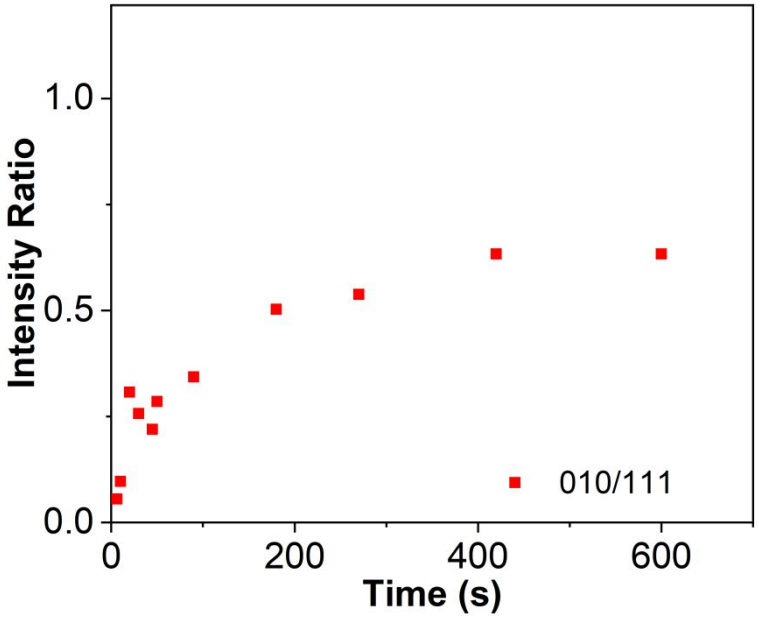

Figure S14. Ratio of (010) and (111) peak intensities for UMCM-1.

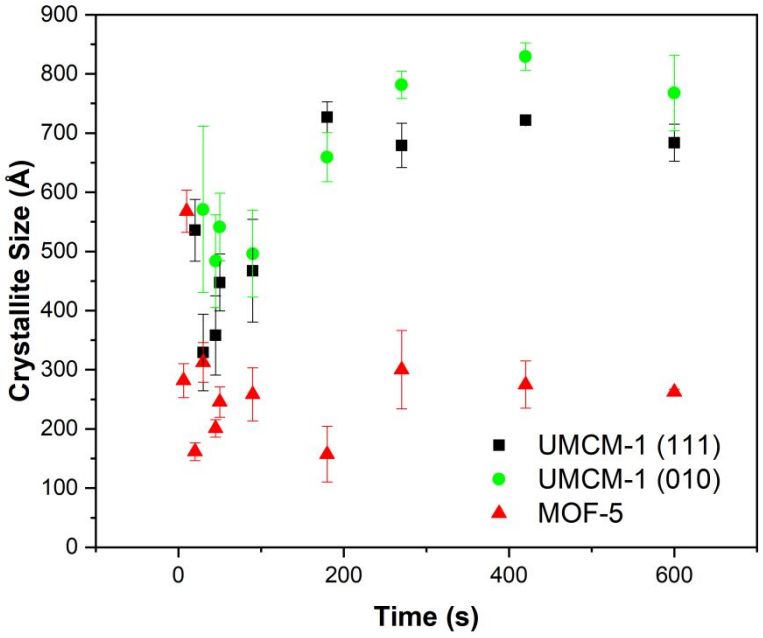

Figure S15. Crystallite size of the two MOF phases as calculated by Scherrer equation using Bragg peaks, UMCM-1 (111), UMCM-1 (010) and MOF-5 (002). Error bars indicate 1 standard deviation.

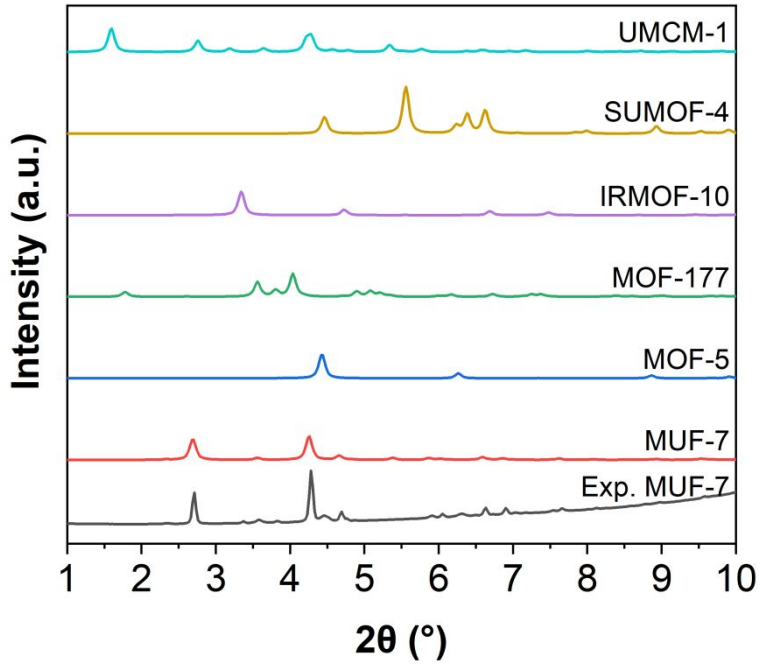

Figure S16. Experimental diffraction pattern compared with potential impurities, MOF-5, MOF-177, IRMOF-10, SUMOF-4 and UMCM-1.

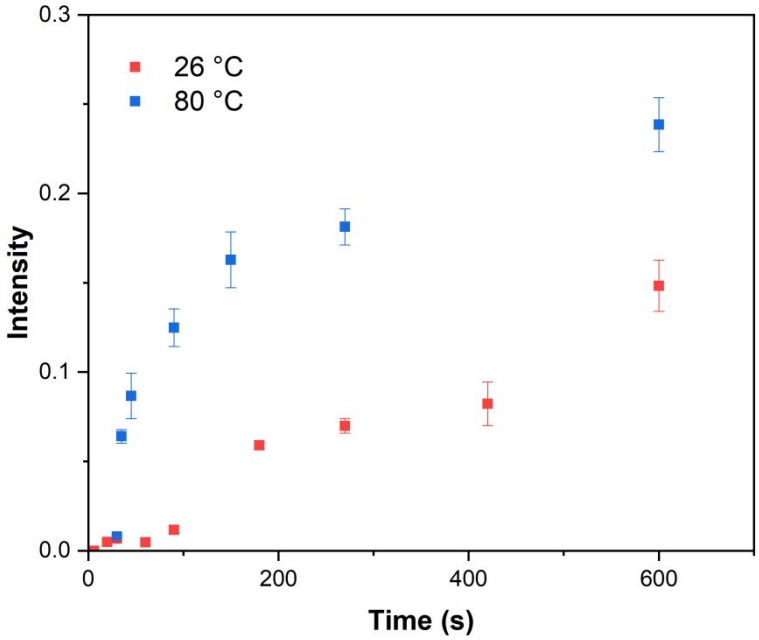

Figure S17. Absolute intensity of the Bragg peak (042) for MUF-7 synthesised at 26 °C and 80 °C. Error bars indicate 1 standard deviation.

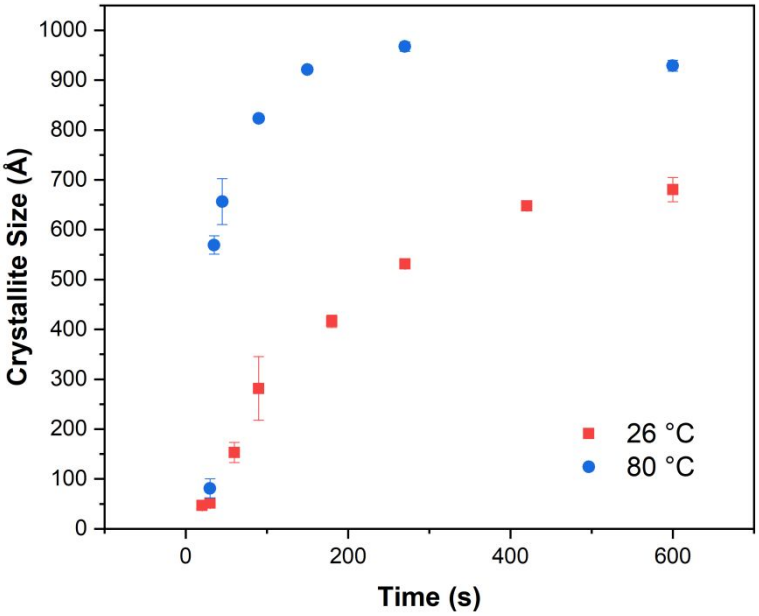

Figure S18. Crystallite size of the MUF-7 synthesised at 26 °C and 80 °C as calculated by Scherrer equation using Bragg peak (042). Error bars indicate 1 standard deviation.

3. 2,3-Dimethylbutane breakthrough experiments

3.1. Preparation of $MgFe_2O_4$@MUF-77-methyl adsorption column

Magnesium ferrite ($MgFe_2O_4$, 0.0129 g) nanoparticles were incorporated with MUF-77-methyl (0.1200 g), synthesised under reaction 3 conditions, to form a 10 wt% loading $MgFe_2O_4$@MUF-77-methyl composite. The preparation was performed through a granulation process whereby the synthesised MUF-77-methyl powder was dispersed in 6 mL of DCM and mixed with the $MgFe_2O_4$ nanoparticle powder. The slurry was then placed under N_2 atmosphere and the solvent was evaporated overnight. The resulting powder was then mixed with a roller mixer for 24 hours to ensure uniform distribution of the two powders. The powder was then dried at 80 °C under vacuum in an oven for 12 hours.

$MgFe_2O_4$@MUF-77-methyl was packed into a borosilicate glass column with glass wool on both ends of the MOF bed to prevent bed movement. Further activation of the adsorbent was performed by flowing N_2 over the bed at a temperature of 66 °C for an hour.

3.1.1. Scanning electron microscopy and energy dispersive X-ray spectroscopy

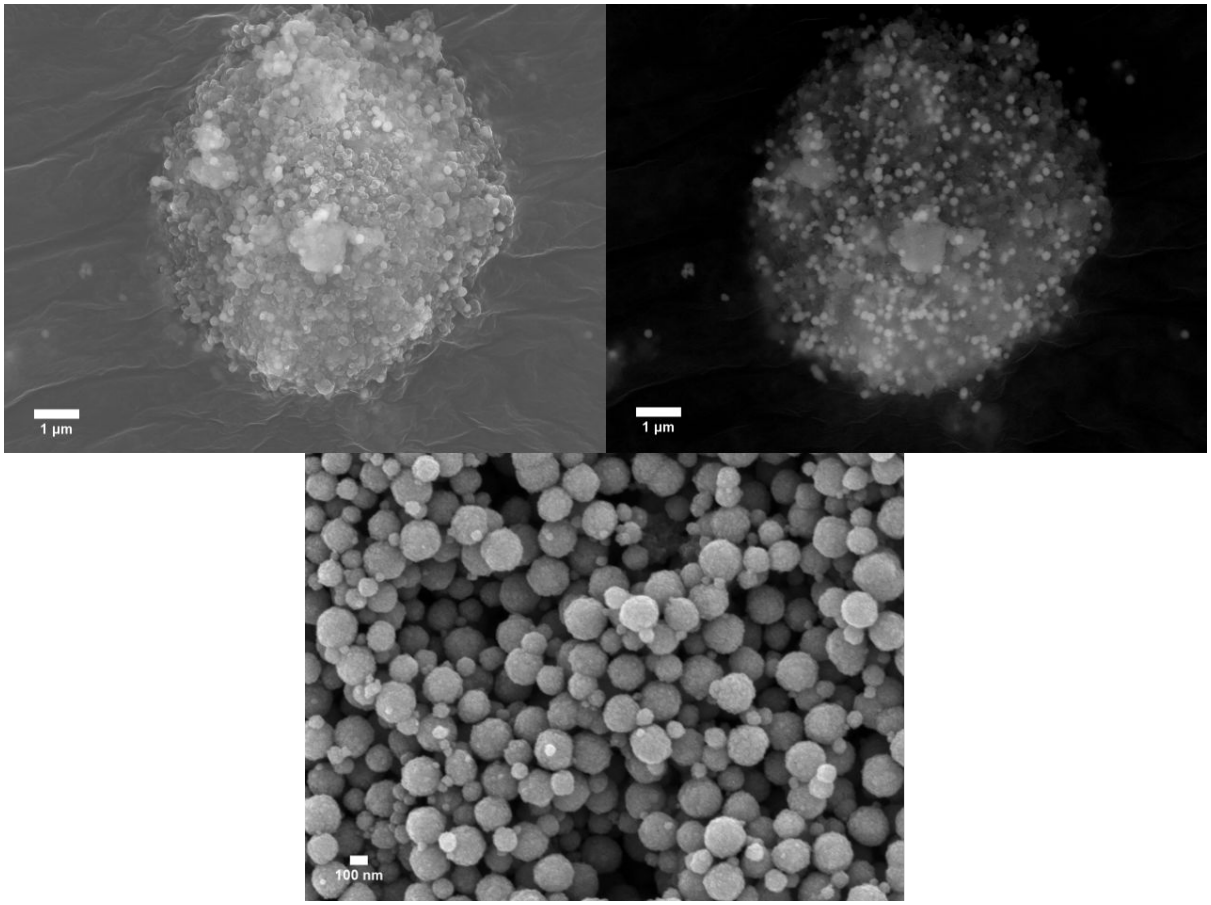

Figure S19. SEM micrographs of (top left) $MgFe_2O_4$@MUF-77-methyl imaged through secondary electrons, (top right) $MgFe_2O_4$@MUF-77 imaged through backscatter electrons, (bottom) $MgFe_2O_4$ imaged through secondary electrons. SEM imaging of $MgFe_2O_4$ shows spherical particles of around 200 nm in size. Secondary electron imaging of the $MgFe_2O_4$@MUF-77-methyl show uniform particle sizes for both the MNPs and the MOF. Backscatter imaging show that the MNPs (bright spots) are well dispersed within the powder matrix of $MgFe_2O_4$@MUF-77-methyl.

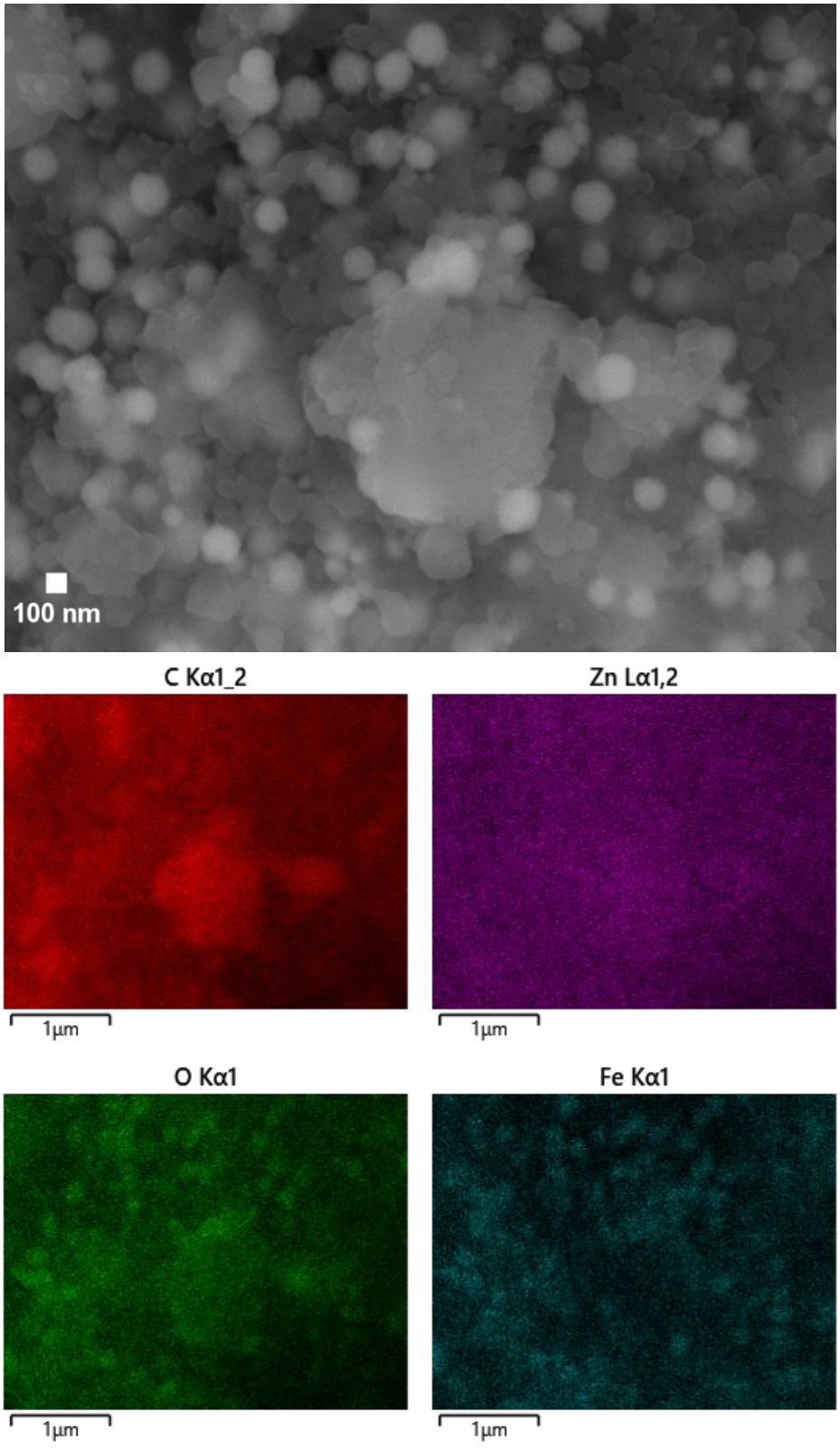

Figure S20. Energy Dispersive X-Ray spectroscopy mapping of the composite powder $MgFe_2O_4$@MUF-77-methyl. Elemental mapping shows the distribution of Fe from $MgFe_2O_4$ compared to Zn and C from MUF-77-methyl. Fe mapping also corresponds to bright spots on backscatter image.

3.1.2. Vibrating sample magnetometry

Vibrating sample magnetometry (VSM) was conducted using RIKEN DENSHI operated at room temperature with a maximum field of 5 kOe. Samples were mounted in a cylindrical sample holder with epoxy resin which was allowed to set and measured.

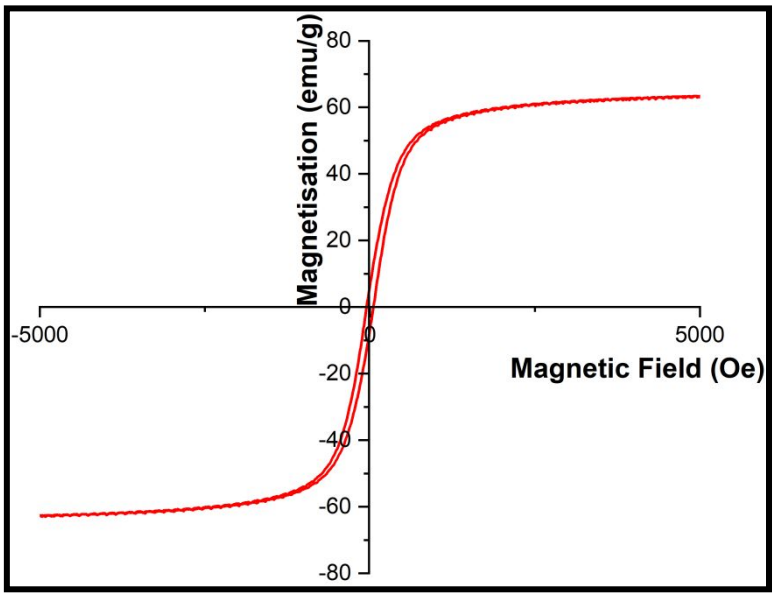

Figure S21. Hysteresis loop of $MgFe_2O_4$.

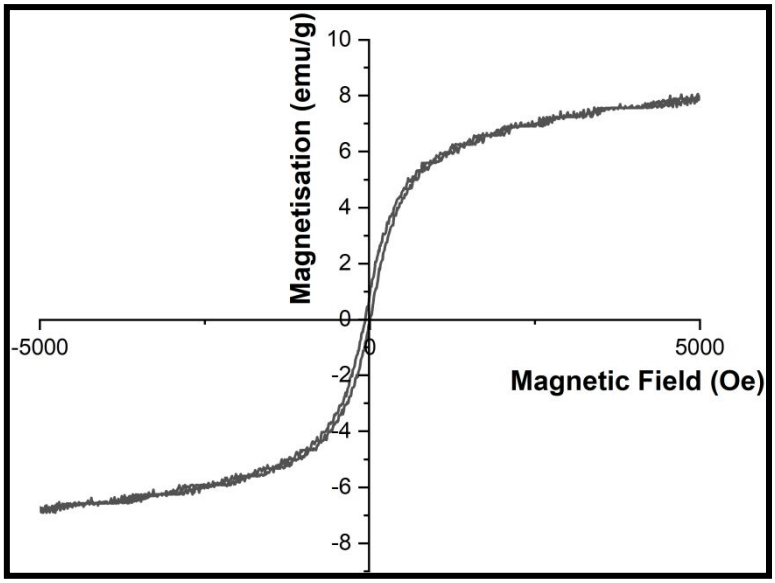

Figure S22. Hysteresis loop of $MgFe_2O_4$@MUF-77-methyl.

3.2. Adsorption experiments

Nitrogen was flowed at 50 mL/min through an enclosed vessel containing 2,3-DMB to deliver the vapour into the adsorption column. The transfer of 2,3-DMB from its container to the enclosed vessel was performed under a N_2 atmosphere to avoid the inclusion of moisture in the adsorption experiments. The vessel temperature was recorded to calculate the vapour pressure of 2,3-DMB through the Antoine equation.

The mass spectrometer, Pfeiffer Vacuum ThermoStar, was calibrated to the vapour pressure as defined by the Antoine equation parameters (**Table S5**) for the bubbler vessel chamber temperature at 20.3 °C.

Antoine equation:

$$\log_{10} P = A - \frac{B}{T + C} \qquad (3)$$

Where P is in mmHg, T is in °C, A, B and C are Antoine equation parameters.

Table S5. Antoine equation parameters for 2,3-Dimethylbutane.[9]

Parameter	Value
A	6.98947
B	1220.01
C	238.956
T_{min} °C	−127.96
T_{max} °C	226.83

Table S6. Breakthrough bed dimensions and packing parameters.

Parameter	Value
Column OD	3/8”
Wall Thickness	2 mm
Bed Height	37 mm
Mass of MOF and Magnetic Nanoparticles	0.1329 g
Mass of MOF	0.1200 g
Packing density	0.1498 g/mm^3

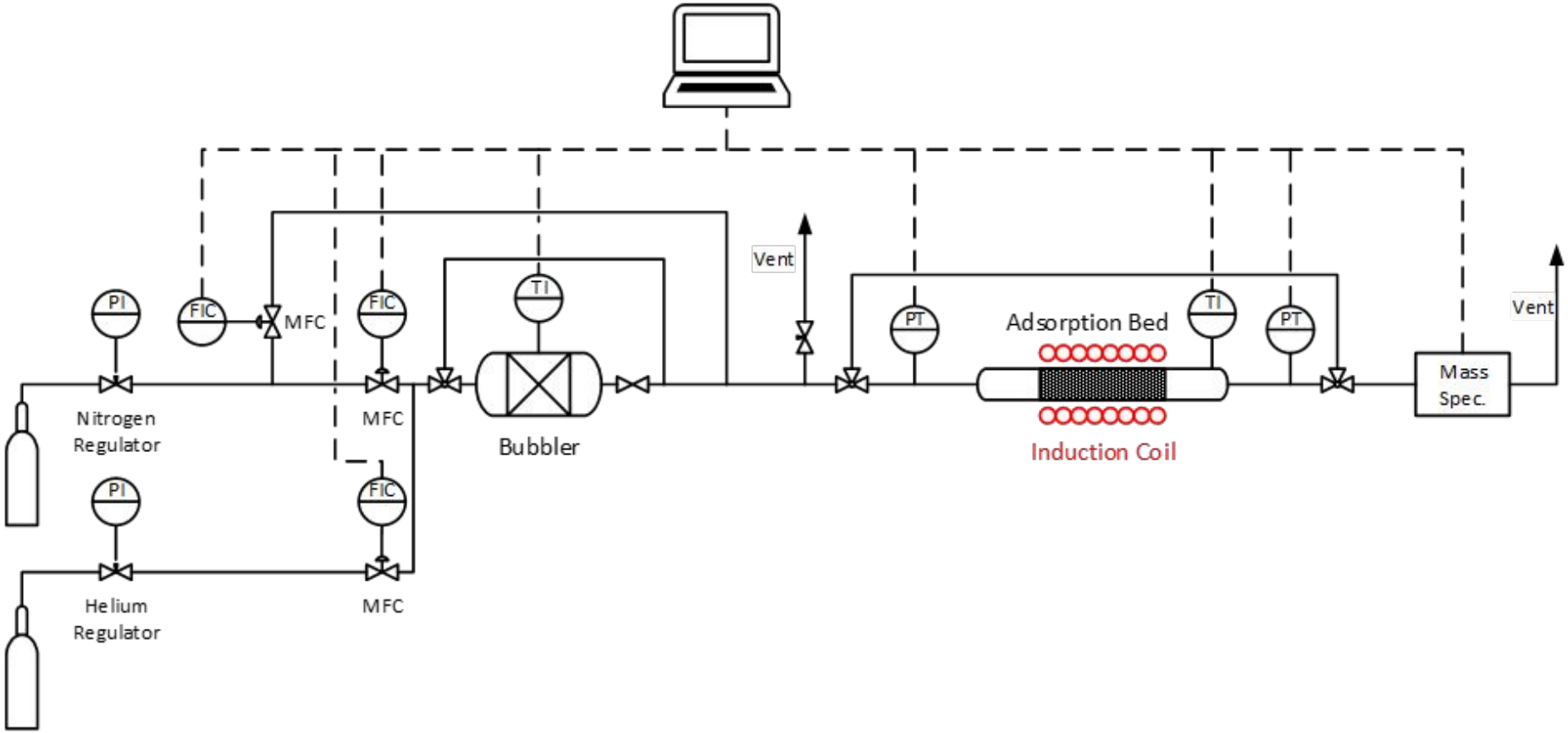

Figure S23. Process Flow Diagram for adsorption bed setup.

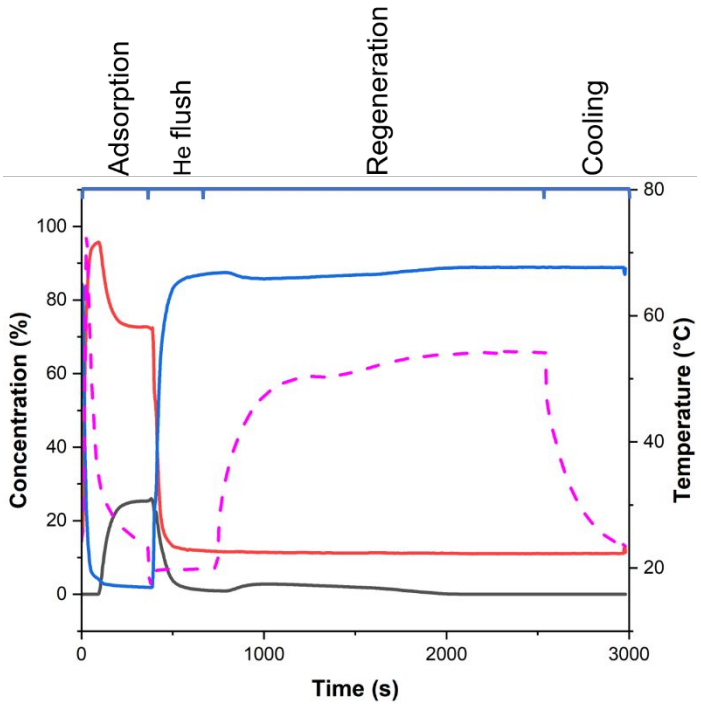

Figure S24. Concentration profile of various components of the feedstream during various phases of adsorption/desorption cycle. (Black) 2,3-Dimethylbutane, (red) nitrogen, (blue) helium. Temperature is shown by the dashed purple line.

3.3. 2,3-Dimethylbutane breakthrough bed capacity calculations

The breakthrough bed capacity calculations were performed over the various stages of the adsorption/desorption cycle.

Firstly, the usable bed capacity is the capacity before breakthrough of adsorbate, where t_b is the time where C/C_0 passes 0.01.

$$t_u = \int_0^{t_b} 1 - \frac{C}{C_0} dt = Area_{usable} \quad (4)$$

Usable bed capacity was calculated from equation 5, where t_b is the time where C/C_0 passes 0.01.

$$Capacity = \frac{Area_{usable} \times \dot{V} \times DMB\ concentration}{Mass\ of\ MOF} \quad (5)$$

The total adsorption capacity includes the usable bed capacity up to the point where the bed is saturated.

$$t_t = \int_0^{\infty} 1 - \frac{C}{C_0} dt = Area_{total} \quad (6)$$

$$Capacity_{total} = \frac{Area_{total} \times \dot{V} \times Concentration_{DMB}}{Mass\ of\ MOF} \quad (7)$$

The regeneration capacity is the amount of 2,3-DMB released during regeneration phase per unit mass of MOF in the bed.

$$Area_{regen} = \int_{t_1}^{t_2} C\ dt \quad (8)$$

$$Regeneration\ amount = Area_{regen} \times \dot{V} \quad (9)$$

$$Capacity_{regen} = \frac{Regen.\ amount}{Mass\ of\ MOF} \quad (10)$$

Table S7. Total adsorption capacity for runs with 3:97 2,3-DMB:N_2 feed concentration.

Run No.	Amount adsorbed (cm^3)	Total adsorption capacity (cm^3/g MOF)
6	15.2	127
7	17.8	148
8	19.1	159

Table S8. Comparison of adsorption capacities of 2,3-dimethylbutane for various adsorbents at vapour pressure of 3 kPa. (*) Denotes capacities obtained from breakthrough experiments conducted at vapour pressures of 6 kPa.

Material	Temperature (K)	Capacity (cm^3/g STP)	Reference
Zeolite BETA	423	10.2	[10]
	473	3.6	[10]
	523	0.9	[10]
UiO-66	343	9.5*	[11]
	373	9.3*	[11]
	423	8.7*	[11]
	473	6.6*	[11]
$Fe_2(BDP)_3$	403	4.3	[12]
	433	1.1	[12]
	473	0.2	[12]
MUF-77	298	275	[2]
CUB-30	298	200	[2]
MUF-77 - Isotherm	298	184	This work
MUF-77 - Breakthrough	293	145	This work

Table S9. Comparison of adsorption capacities of 2,3-dimethylbutane for various adsorbents at vapour pressure of 25 kPa.

Material	Temperature (K)	Capacity (cm^3/g STP)	Reference
Zeolite BETA	423	17.8	[10]
	473	9.8	[10]
	523	4.1	[10]
$Fe_2(BDP)_3$	403	17.9	[12]
	433	6.5	[12]
	473	1.6	[12]
MUF-77	298	294	[2]
CUB-30	298	220	[2]
MUF-77 - Isotherm	298	200	This work
MUF-77 - Breakthrough	293	176	This work

4. References

1. Liu, L.; Telfer, S. G., Systematic Ligand Modulation Enhances the Moisture Stability and Gas Sorption Characteristics of Quaternary Metal-Organic Frameworks. *J. Am. Chem. Soc.* **2015,** *137* (11), 3901–3909.
2. Macreadie, L. K.; Babarao, R.; Setter, C. J.; Lee, S. J.; Qazvini, O. T.; Seeber, A. J.; Tsanaktsidis, J.; Telfer, S. G.; Batten, S. R.; Hill, M. R., Enhancing Multicomponent Metal-Organic Frameworks for Low Pressure Liquid Organic Hydrogen Carrier Separations. *Angew Chem Int Ed* **2020,** *59* (15), 6090–6098.
3. Hashemzadeh, A.; Amini, M. M.; Khavasi, H. R.; Ng, S. W., Ligand Preferences in Ytterbium Ions Complexation with Carboxylate-Based Metal-Organic Frameworks. *J. Coord. Chem.* **2017,** *70* (18), 3217–3232.
4. Deng, H.; Li, X.; Peng, Q.; Wang, X.; Chen, J.; Li, Y., Monodisperse Magnetic Single-Crystal Ferrite Microspheres. *Angew. Chem.* **2005,** *117* (18), 2842–2845.
5. Avrami, M., Kinetics of Phase Change. I General Theory. *J. Chem. Phys.* **1939,** *7* (12), 1103–1112.
6. Avrami, M., Kinetics of Phase Change. II Transformation-Time Relations for Random Distribution of Nuclei. *J. Chem. Phys.* **1940,** *8* (2), 212–224.
7. Avrami, M., Granulation, Phase Change, and Microstructure Kinetics of Phase Change. III. *J. Chem. Phys.* **1941,** *9* (2), 177–184.
8. Jensen, K. M.; Tyrsted, C.; Bremholm, M.; Iversen, B. B., In Situ Studies of Solvothermal Synthesis of Energy Materials. *ChemSusChem* **2014,** *7* (6), 1594–1611.
9. Yaws, C. L.; Narasimhan, P. K.; Gabbula, C., Vapor Pressure of Organic Compounds. In *Yaws' Handbook of Antoine Coefficients for Vapor Pressure (2nd Electronic Edition)*, Knovel.
10. Bárcia, P. S.; Silva, J. A. C.; Rodrigues, A. E., Multicomponent Sorption of Hexane Isomers in Zeolite Beta. *AlChE J.* **2007,** *53* (8), 1970–1981.
11. Bárcia, P. S.; Guimarães, D.; Mendes, P. A. P.; Silva, J. A. C.; Guillerm, V.; Chevreau, H.; Serre, C.; Rodrigues, A. E., Reverse Shape Selectivity in the Adsorption of Hexane and Xylene Isomers in MOF UiO-66. *Microporous Mesoporous Mater.* **2011,** *139* (1-3), 67–73.
12. Herm, Z. R.; Wiers, B. M.; Mason, J. A.; van Baten, J. M.; Hudson, M. R.; Zajdel, P.; Brown, C. M.; Masciocchi, N.; Krishna, R.; Long, J. R., Separation of Hexane Isomers in a Metal-Organic Framework with Triangular Channels. *Science* **2013,** *340* (6135), 960–964.